Sediments of Lake Vens (SW European Alps, France) record large-magnitude earthquake events

Jade Petersen, Bruno Wilhelm, Marie Revel, Yann Rolland, Christian Crouzet, Fabien Arnaud, Elodie Brisset, Eric Chaumillon, Olivier Magand

▶ **To cite this version:**

Jade Petersen, Bruno Wilhelm, Marie Revel, Yann Rolland, Christian Crouzet, et al.. Sediments of Lake Vens (SW European Alps, France) record large-magnitude earthquake events. Journal of Paleolimnology, 2014, 51, pp. 343-355. 10.1007/s10933-013-9759-x . halsde-00976088

HAL Id: halsde-00976088
https://hal.science/halsde-00976088

Submitted on 30 Apr 2020

HAL is a multi-disciplinary open access archive for the deposit and dissemination of scientific research documents, whether they are published or not. The documents may come from teaching and research institutions in France or abroad, or from public or private research centers.

L'archive ouverte pluridisciplinaire **HAL**, est destinée au dépôt et à la diffusion de documents scientifiques de niveau recherche, publiés ou non, émanant des établissements d'enseignement et de recherche français ou étrangers, des laboratoires publics ou privés.

Sediments of Lake Vens (SW European Alps, France) record large-magnitude earthquake events

Jade Petersen · Bruno Wilhelm · Marie Revel · Yann Rolland · Christian Crouzet · Fabien Arnaud · Elodie Brisset · Eric Chaumillon · Olivier Magand

Abstract We studied sediment cores from Lake Vens (2,327 m asl), in the Tinée Valley of the SW Alps, to test the paleoseismic archive potential of the lake sediments in this particularly earthquake-sensitive area. The historical earthquake catalogue shows that moderate to strong earthquakes, with intensities of IX–X, have impacted the Southern Alps during the last millennium. Sedimentological (X-ray images, grain size distribution) and geochemical (major elements and organic matter) analyses show that Lake Vens sediments consist of a terrigenous, silty material (minerals and organic matter) sourced from the watershed and diatom frustules. A combination of X-ray images, grain-size distribution, major elements and magnetic properties shows the presence of six homogenite-type deposits interbedded in the sedimentary background. These sedimentological features are ascribed to sediment reworking and grain sorting caused by earthquake-generated seiches. The presence of microfaults that cross-cut the sediment supports the hypothesis of seismic deposits in this system. A preliminary sediment chronology is provided by ^{210}Pb measurement and AMS ^{14}C ages. According to the chronology, the most recent homogenite events are attributable to damaging historic earthquakes in AD 1887 (Ligure) and 1564 (Roquebillière). Hence, the Lake Vens sediment recorded large-magnitude

J. Petersen · B. Wilhelm · M. Revel (✉) · Y. Rolland
CNRS, IRD, Observatoire de la Côte d'Azur, Géoazur UMR 7329, Nice Sophia Antipolis University, 250 rue Albert Einstein, Sophia Antipolis, 06560 Valbonne, France
e-mail: revel@geoazur.unice.fr

J. Petersen · E. Brisset
CNRS, IRD, Collège de France, UM 34 CEREGE, Aix-Marseille University, Technopôle de l'Arbois, BP 80, 13545 Aix-en-Provence cedex 04, France

C. Crouzet
CNRS, ISTerre Université de Savoie, Bâtiment Belledonne, 73376 Le Bourget du Lac, France

F. Arnaud
Laboratoire Environnement Dynamique et Territoire de Montagne, CNRS, Université de Savoie, Pôle Montagne, 73376 Le Bourget du Lac, France

E. Brisset
UMR 7263, IMBE, Technopôle de l'Arbois, BP 80, 13545 Aix-en-Provence cedex 04, France

E. Chaumillon
UMR CNRS 7266 LIENSs, Université de La Rochelle, 2 rue Olympe de Gouges, 17000 La Rochelle, France

O. Magand
LGGE, Laboratoire de Glaciologie et Géophysique de l'Environnement, CNRS, UJF–Grenoble 1, 38041 Grenoble, France

earthquakes in the region and permits a preliminary estimate of recurrence time for such events of ~400 years.

Keywords Homogenites · Paleo-earthquakes · Lake sediments · High altitude · SW European Alps

Introduction

For several decades, lacustrine sediments have been recognized as recorders of earthquakes in seismically active areas (Seilacher 1969; Beck et al. 1996; Chapron et al. 1999; Alfaro et al. 1999; Rodriguez-Pascua et al. 2000; Arnaud et al. 2002; Strasser et al. 2006; Wilhelm et al. 2013). Establishment of a detailed chronology of earthquakes in seismically active areas is a critical objective to estimate the recurrence time of high-magnitude events. Earthquakes can be recorded in lacustrine sediments by different types of deposits, such as debris flows (Arnaud et al. 2002; Nomade et al. 2005; Strasser et al. 2006), turbidites (Shiki et al. 2000; Strasser et al. 2006), homogenites (Chapron et al. 1999; Beck 2009) or deformation structures like liquefaction structures or microfaults (Beck et al. 1996; Monecke et al. 2004). Whatever the form, formation and preservation of earthquake records in lacustrine sediments depends on several factors (Sims 1973, 1975): (1) the nature of the sediment, mainly its water content and grain size (Plaziat and Ahmamou 1998; Jewell and Ettensohn 2004; Monecke et al. 2004), (2) distance from the epicenter (Ambraseys 1988; Obermeier 1996; Strasser et al. 2006) and (3) earthquake magnitude (Rodriguez-Pascua et al. 2000).

This paper presents results from a multi-proxy study of sediment cores from Lake Vens, located in an area subject to ongoing seismic activity, in the southwestern Alps. The active Jausiers-Tinée fault is about 2 km NW of the lake, which is characterized by a swarm of microseismicity (Jenatton et al. 2007) and Quaternary tectonic offsets of geomorphology (Sanchez et al. 2010a, 2010b; Darnault et al. 2012). The main objective of this study was to test if historically documented macro-seismic events were recorded by the Lake Vens sediments. If Lake Vens sediment proves to record earthquakes, it will be a useful tool for paleoseismic documentation of major earthquake recurrence during the Holocene.

Regional seismic hazard and vulnerability

The Alpes Maritimes is one of the most seismically active regions in the southwestern Alps, characterized by historical $Mw > 6$ and ongoing $Mw < 4$ earthquakes (Courboulex et al. 2003). The most damaging known event was the AD 1564 Roquebillière earthquake, with an estimated maximum epicentre MSK intensity of IX–X (Boschi et al. 1997; Lambert and Levret 1996; Laurenti 1998). Such strong earthquakes are considered to have recurrence intervals of hundreds to thousands of years (GEMEP 2005). These seismogenic hazards produce high risk because of the dense urbanization of the Mediterranean coast. Previous mapping studies and monitoring of seismic activity over 30 years identified many active faults (Courboulex et al. 2003; Sanchez et al. 2010a, 2010b; Larroque et al. 2011; Bauve et al. 2012). Vulnerability analysis, mainly for the city of Nice and its surroundings, has been undertaken in recent years, and is already acknowledged by several organizations such as the BRGM (Bureau des Recherches Géologiques et Minières), the IRSN (Institut de Radioprotection et de Sûreté Nucléaire) and the CETE (Centre d'Études Techniques de l'Équipement) for risk assessment. Monitoring of seismic activity, however, does not enable the estimation of recurrence time for large seismic events, which may be >1 ka. Hence, the historic earthquake record is not long enough to determine the frequency of large-magnitude events. Therefore, geological archives such as lake sediments must be investigated to produce reliable seismic-hazard and related risk assessments.

Lake Vens geological context

Lake Vens (44°18′40N, 6°55′56E, 2,327 m asl) is located in the Argentera-Mercantour massif along the Tinée Valley (Alpes Maritimes, France), in the southwestern Alps (Fig. 1a). This high-altitude massif is composed mainly of Hercynian crystalline rocks (granite and gneiss), affected by strong localized deformations in narrow fault corridors. This deformation is linked to the formation of the Alpine chain (Sanchez et al. 2011a, 2010b) and it is currently

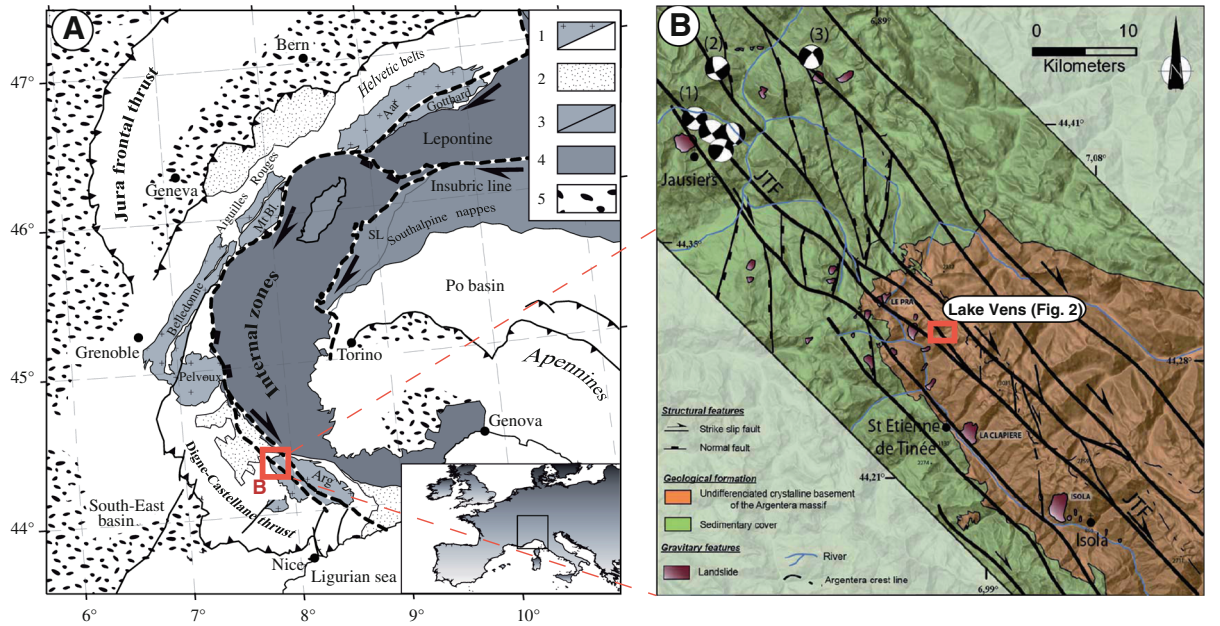

Fig. 1 **a** Schematic geological map of the western Alps, with location of the study area (**b** enlarged on the *left*). External Alps comprise: (*1*) Hercynian crystalline basement (crosses) and its autochthonous Mesozoic sedimentary cover (white); (*2*) The transported klippes of Helminthoid Upper Cretaceous flysh and Internal Briançonnais and Penninic units. Internal Alps comprise: (*3*) Briançonnais and Piemontais zones, which are made of variably metamorphosed rocks from the continental European margin and the Alpine Tethys oceanic domain; (*4*) the Austro-Alpine units comprising the Dent Blanche klippe and the Apulian margin. (*5*) Molasse sediments deposited during the Oligocene to Pliocene lie in the periphery of the Alps. **b** Simplified structural map of the northwest part of the Argentera-Mercantour massif (after Sanchez et al. 2010a, b, 2011a, b). The red frame shows the location of Lake Vens, the map of which is displayed in Fig. 2. Focal mechanisms highlight (*1*) the seismic swarm of the 2003–2004 Jausiers Seismic crisis, (*2*) earthquake of 26 February 2012 (Mw: 4.7) and (*3*) earthquake of 1959 (Mw: 5.5)

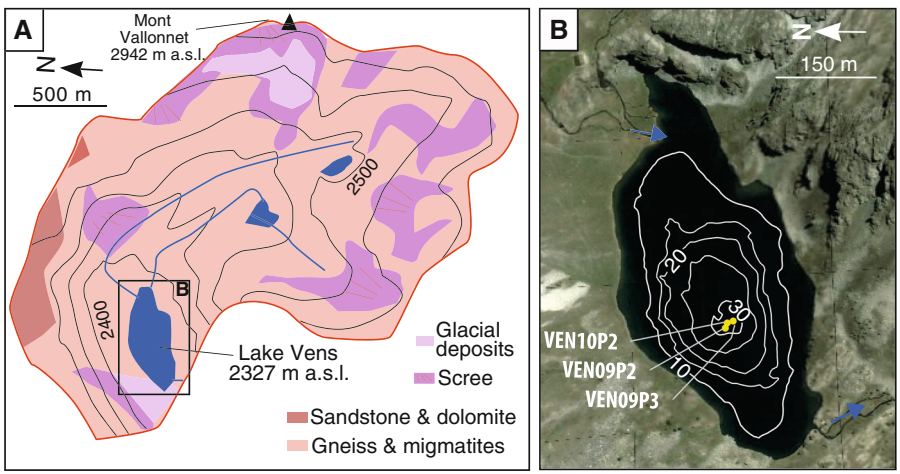

Fig. 2 **a** Geological and geomorphological characteristics of the Lake Vens catchment (2,300 m asl) **b** Bathymetric map of the lake and location of the VEN09P3, VEN09P2 and VEN10P2 cores

responsible for ongoing seismicity, especially in the Jausiers-Tinée area (Jenatton et al. 2007; Sanchez et al. 2010a, b) (Fig. 1b). One of main faults passes several hundred meters south of Lake Vens and offsets Quaternary morphologies (crests and glacier-polished surfaces) by 5–50 m (Fig. 1b).

The catchment area of Lake Vens is 4 km^2 and its geology is composed mainly of gneiss, with only

minor presence of sedimentary rocks (sandstone and dolomite) (Fig. 2a). Because of the high elevation, the catchment is covered by sparse grassy vegetation, and by snow from November to May. During this period, the lake's surface is frozen and, hence, sediment input occurs mainly during summer and early autumn. At this high elevation and given the Mediterranean climate, spring, summer and autumn floods control lake-watershed hydrology, a consequence of snow-melt and abundant rainfall. Two tributaries drain the catchment area and enter the east side of the lake (Fig. 2b). The lake is 270 m wide, 600 m long, has an area of 0.1 km^2 and is composed of two main sedimentary sub-basins. The smaller sub-basin is located in the eastern part of the lake in front of the delta and corresponds to a platform at 15 m maximum depth. The main sub-basin is located at the centre of the lake and has a maximum depth of 32 m.

Materials and methods

Coring

In 2009 and 2010, we used a gravity corer to retrieve three sediment cores (VEN09P3, VEN09P2 and VEN10P2), 168, 152 and 51 cm long, respectively. Cores were collected from the deepest sub-basin (Fig. 2b).

Sedimentology and geochemistry

Scopix X-ray spectrometry, coupled to an image intensifier and a 16-bit CCD camera (Bordeaux University), was used to study the sedimentary structure of VEN09P3. Variables such as lithology, grain size, water content, porosity and compaction control the X-ray response (Migeon et al. 1999). Major elements were semi-quantitatively determined at 1-mm resolution by X-ray fluorescence (XRF) spectrometry using an Avaatech XRF Core Scanner at Bordeaux University. Grain size of VEN09P3 was measured with a Coulter LS200 laser-diffraction particle analyzer at the Geoazur Laboratory (Nice, Sophia Antipolis University), using a 5-mm sampling step. Organic geochemistry was determined at a sampling step of 5 cm, using a Rock–Eval pyrolyser (Orléans University). Hydrogen Index (HI) and Oxygen Index (OI) were calculated from the assessment of the Total Organic Content (TOC) and its temperature peak during pyrolysis (S2 and S3), following Meyers and Lallier-Vergès (1999) and Disnar et al. (2003). HI represents the quantity of hydrocarbon products rejected during the pyrolysis, whereas OI is linked to oxygen quantity.

Magnetic properties

To identify homogenite-type deposits that might be related to paleo-earthquakes, measures of several magnetic variables were made following the method of Campos et al. (2013). Seventy-eight cubic sub-samples (edge = 2.1 cm) and a U-channel (1.5 m long) were collected from core VEN09P2 to measure anisotropy of magnetic susceptibility and remanent magnetization. All magnetic measurements were carried out in the CEREGE Laboratory of Magnetism (Aix-Marseille University). The AGICO MFK1-FA Kappabridge (spinning method) was used for measurements of anisotropy of magnetic susceptibility. To identify magnetism-carrying particles and possible impact on anisotropy of magnetic susceptibility, laboratory Isothermal and Anhysteretic Remanent Magnetizations (IRM and ARM, respectively) were imparted and then demagnetized using alternative field (AF) (Campos et al. 2013). Remanent magnetizations were measured after each AF step using a superconducting quantum interference device (SQUID) pass-through magnetometer (2G 760R), located in a shielded room.

Chronology

The uppermost 21 cm of the VEN09P3 sediment core were sampled following a regular 1-cm sampling step for radionuclide measurements. Activity of ^{210}Pb was measured by gamma spectrometry at the Laboratory of Glaciology and Geophysics of the Environment (LGGE), following the initial procedure described by Gaggeler et al. (1976). The ^{210}Pb was used to determine sedimentation rate over the last century. Excess ^{210}Pb at each depth was calculated as the difference between total ^{210}Pb and ^{226}Ra activity. We then applied the Constant Flux/Constant Sedimentation (CFCS) model to the excess ^{210}Pb distribution to calculate dates and sedimentation rates (Goldberg 1963).

Five samples of undifferentiated terrestrial vegetal remains were selected for AMS ^{14}C analysis at the

Table 1 VEN09P3 and VEN10P2 core radiocarbon chronology

Code lab	Core	Core depth (cm)	Composite depth (cm) for VEN09P3	Material	Age 14C AMS conv. BP	Date error	Cal. years BP (±2 sigmas)
SacA22282	*VEN09P3*	*38*	*31*	*Vegetal remains undiff.*	*470*	*30*	*495–540*
Poz34153	VEN09P3	93	72.5	Vegetal remains undiff.	1,155	30	980–1,171
SacA22284	VEN09P3	153	111.5	Vegetal remains undiff.	2,470	30	2,365–2,711
SacA31217	*VEN10P2*	*37*	*25.5*	*Coleopter remains*	*355*	*45*	*313–497*
SacA28193	VEN10P2	42	27.5	Vegetal remains undiff.	300	30	297–459

Radiocarbon dating was performed at the Laboratoire de Mesure du Carbone 14-Saclay by the national facility LM14C in the framework of INSU ARTEMIS call-for-proposal and Poznań Radiocarbon Laboratory. The composite depth was calculated by removing the six H layers, which correspond to instantaneous deposits. See text for explanations on the nature of samples and the calibration procedures. Rejected dates are indicated in italics

French national facility LMC14 (UMS 2572) at Saclay and Poznań Radiocarbon Laboratory (Table 1). ^{14}C ages were calibrated using the Intcal09 calibration curve (Reimer et al. 2009; Table 1) and an age model was generated using the R-code package "clam" (Blaauw 2010).

Results

Sedimentological and geochemical features of Lake Vens sediments

Sediment facies were defined using both macroscopic visual observation and X-ray images (Fig. 3). The sediment is composed of irregular, mm-scale laminae, in which eight to ten homogenous deposits are interbedded (grey patterns in Fig. 3). Among them, two homogenous deposits are highlighted by bright X-ray images at 40-55 and 120-130 cm depth in VEN09P3. Brighter colour indicates less dense sediments (Migeon et al. 1999) for these two layers designated D1 and D2, respectively. By contrast, six homogenous deposits appear opaque, and hence denser, in the X-ray images at depths of 11–13, 32–38, 81–84, 86–95, 104–110 and 141–153 cm. They are designated H1, H2, H3, H4, H5 and H6, respectively. Two additional deposits appear opaque at depths of 7–8 and 17–18 cm. They are, however, too thin to allow identification of the homogenous characteristic of the thicker H layers. X-ray images also revealed four microfaults (>1 cm) between 78 and 118 cm depth. The grain-size distribution curve indicates two dominant modes, at 40 and 150 µm. Based on observations of smear slides, the 40-µm mode corresponds mainly to mineral fragments such as quartz, mica and feldspar, and the detrital fraction weathered from the basement gneiss in the catchment and delivered to the lake by river inflow. The abundant 150-µm fraction is composed mainly of centric diatom frustules (single diatom diameter around 150 µm, colony length to 2 mm). This mode is particularly well represented in the D layers, in which diatoms were notably abundant in smear slides. Furthermore, H layers show specific grain-size features, particularly in the thickest layers (H2, H4, H5 and H6), with (1) a coarse base (Q50 > 60 µm) of <1 cm (red curves in the frequency distribution curve, Fig. 3) because of a dominant sandy mineral fraction, (2) a main layer characterized by homogenous grain size and (3) a fine, whitish clay cap on the top of the homogenous layer of <1 cm (blue curves in the frequency distribution curve, Fig. 3).

The plot of Si/K versus Ca/K (Fig. 4) displays a negative correlation, suggesting that the sediment of Lake Vens is mainly made up of biogenic silica, in particular diatom frustules, and river-borne lithogenic material. Si/K is thus an appropriate geochemical proxy to highlight variability in diatom abundance throughout the core (Fig. 5). The Si/K ratio is < 1 throughout the entire core, except in the D1 and D2 layers (Fig. 5). This pattern is in agreement with the increase in observable diatoms (Fig. 4). In contrast, Ca/K is unrelated to any biogenic fraction, because neither ostracods nor limestone fragments, as revealed by negative HCl tests, are observed in smear slides. Enrichment in Ca is ascribed to the terrigenous fraction, constituted by plagioclase feldspar, whereas K is present in two micas, biotite and muscovite. Consequently, mm-scale Ca/K variability could be

Sediment depth (cm)
0 10 20 30 40 50 60 70 80 90 100 110 120 130 140 150 160 170
VEN10P2
Photo
H1
H2
355 ± 45 yr BP
300 ± 30 yr BP
VEN09P2
Foliation
Photo
H1
H2
D1
H3
H4
H5
D2
H6
1 1.02 1.04 1.06
VEN09P3
Grain-size
X-ray images
Photo
H?
H?
<3.9 µm
<63 µm
<125 µm
<250 µm
<500 µm
<900 µm
Micro-fault
Micro-fault
0 80
Q50 (µm)
µm 1 10 10² 10³ 0 100%
40 µm
150 µm
400 µm
470 ± 30 yr BP
1155 ± 30 yr BP
2470 ± 30 yr BP
Sediment depth (cm)

◀**Fig. 3** Sedimentological features (X-ray images and grain size) of the VEN09P3 core, foliation parameter of the VEN09P2 core and stratigraphic correlation between the VEN09P3, VEN09P2 and VEN10P2 (photo before and after oxidation) cores. For the frequency curve of the VEN09P3 grain size, the *blue lines* emphasize the top of the H layers (fine mode) and the *red lines* emphasize the bottom (coarse mode). Homogenous deposits are called H and D. Enlargement of the microfaults is shown in *red*. ^{14}C-date depths from the VEN09P3 and VEN10P2 cores are indicated by *white stars*

related to grain-size distribution resulting from changes in transport energy (Wilhelm et al. 2012a). The most striking geochemical feature is the almost constant Ca/K ratio observed in the H layers (Fig. 5).

Increases in sulphur and TOC are documented in the two D layers (5 % TOC in D1 and 7 % TOC in D2). In contrast, sulphur and TOC (<2 %) contents are low in the six H layers. In the HI versus OI diagram (Fig. 6), samples are distributed between type II (algal) and type III (vascular plant) organic matter as defined by Espitalie et al. (1985) in Meyers and Lallier-Vergès (1999). Hence, the D layers appear to be enriched in autochthonous organic matter, whereas the organic-poor H layers appear to contain mainly allochthonous organic matter.

Magnetic properties

The minimum axes of the anisotropy of magnetic susceptibility are well grouped and present an average inclination of 73.1° ± 5.8°. The clustering of the minimum axis, close to the vertical, implies good preservation of primary sedimentary structures. Only a few samples in the uppermost part of the core deviate from this average, probably because of their high water content, which makes good preservation of structures during the coring and/or sub-sampling processes very difficult. As a result, samples from the uppermost part of the core were not considered in this study.

Laboratory remanent magnetization analyses show a very constant mean destructive field of 36 ± 3 and 34 ± 2 mT for ARM and IRM, respectively. It implies that magnetic mineralogy is constant and dominated by magnetite. Variations in the intensity of ARM and IRM are probably a consequence of small changes in the amount of magnetite in the sediment. No clear relation between variation of magnetization parameters and the foliation parameter of the anisotropy of magnetic susceptibility (F) was observed. Therefore, the shape of the anisotropy of magnetic susceptibility ellipsoid is probably caused by the orientation of clay minerals.

In the studied section, the lineation parameter of the anisotropy of magnetic susceptibility is relatively low and constant (1.009 ± 0.007), whereas the F parameter shows low values (1.014 ± 0.009), except in the H layers, where values are >1.02 (Fig. 3). Large variations and anomalously high F values with respect

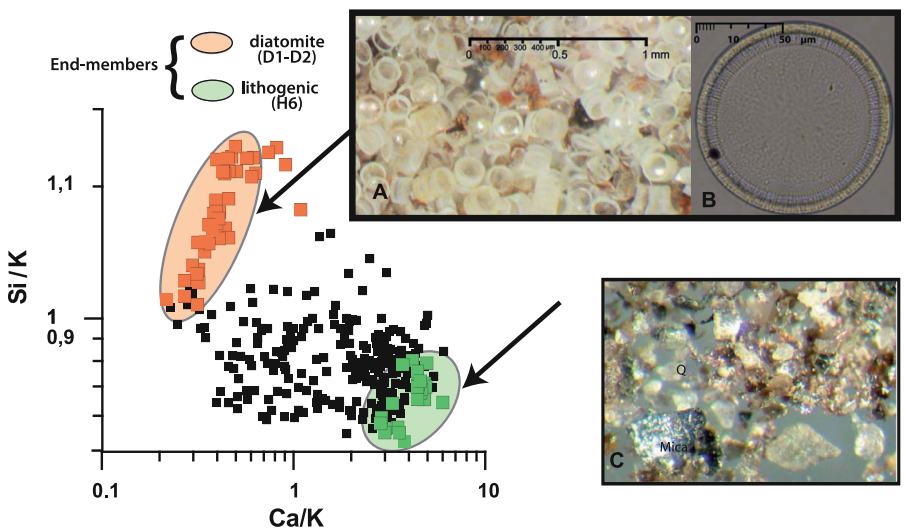

Fig. 4 Si/K versus Ca/K ratios. Data scatter reflects mixing of two end-members in various proportions: (1) authigenic source (diatoms) and (2) detrital input from eroded crystalline basement in the watershed. **a** View of diatomite in the sediment. **b** Single diatom. C. Smear slide at 91 cm depth, showing the lithogenic fraction (mica and quartz)

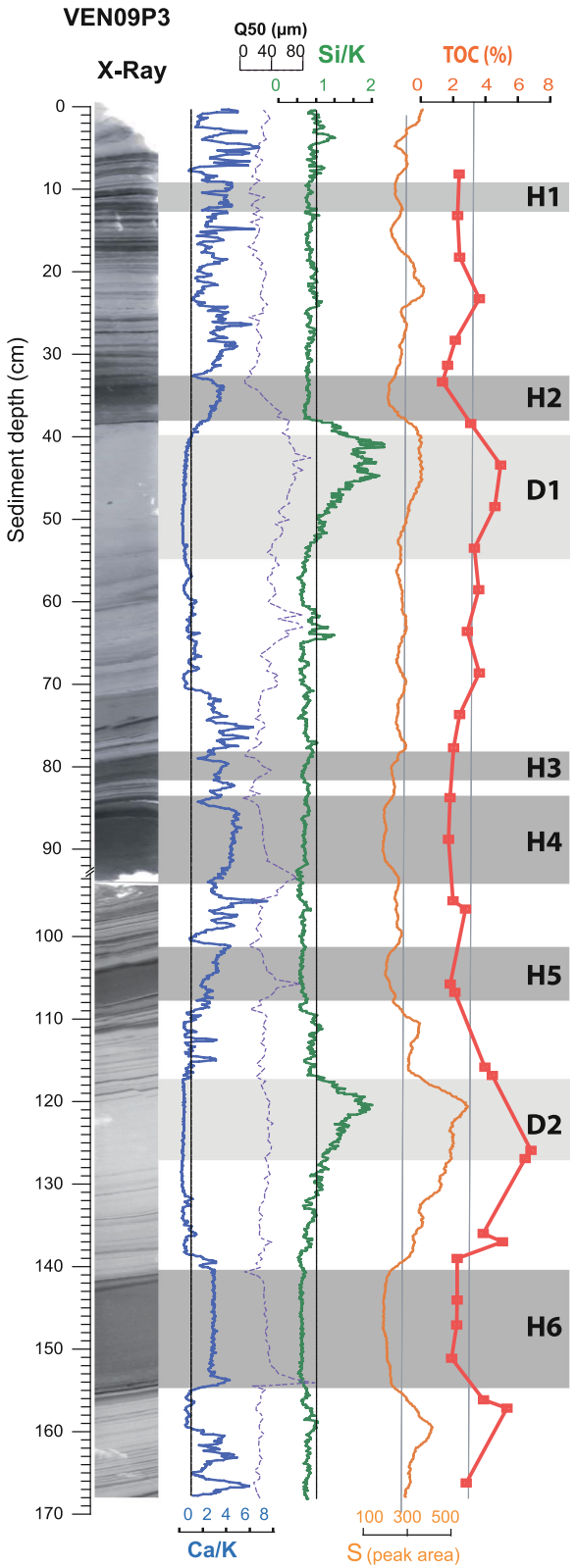

◀ **Fig. 5** Geochemical features of the VEN09P3 core: X-ray images, Ca/K ratios, grain size (Q50), Si/K ratios, S content and organic matter (TOC) content versus depth (cm), indicating the main sedimentary facies (D and H layers)

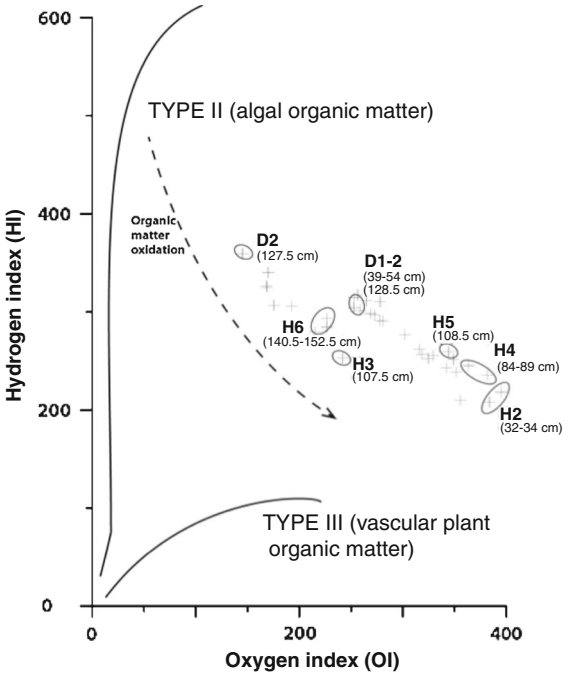

Fig. 6 Hydrogen Index versus Oxygen Index diagram for core VEN09P3 sediments. Samples from the H and D layers are circled. Organic matter type II and III patterns are indicated

to compaction have been highlighted previously by several authors and interpreted as being a consequence of oscillations in the mass of water during the slow decantation of re-suspended material (Beck 2009; Campos et al. 2013).

Chronology

The excess ^{210}Pb profile for core VEN09P3 shows a regular decrease from 887 ± 57 Bq kg^{-1} at the top of core to 26 ± 8 Bq kg^{-1} at 8.5 cm depth, with mean uncertainty of about 21 % (Fig. 7a). Below 8.5 cm, uncertainties are in the range of the measured values; these deeper samples were thus not considered for the application of the CFCS model. The CFCS model (Goldberg 1963) yielded an estimated linear sedimentation rate of 0.7 ± 0.1 mm/year.

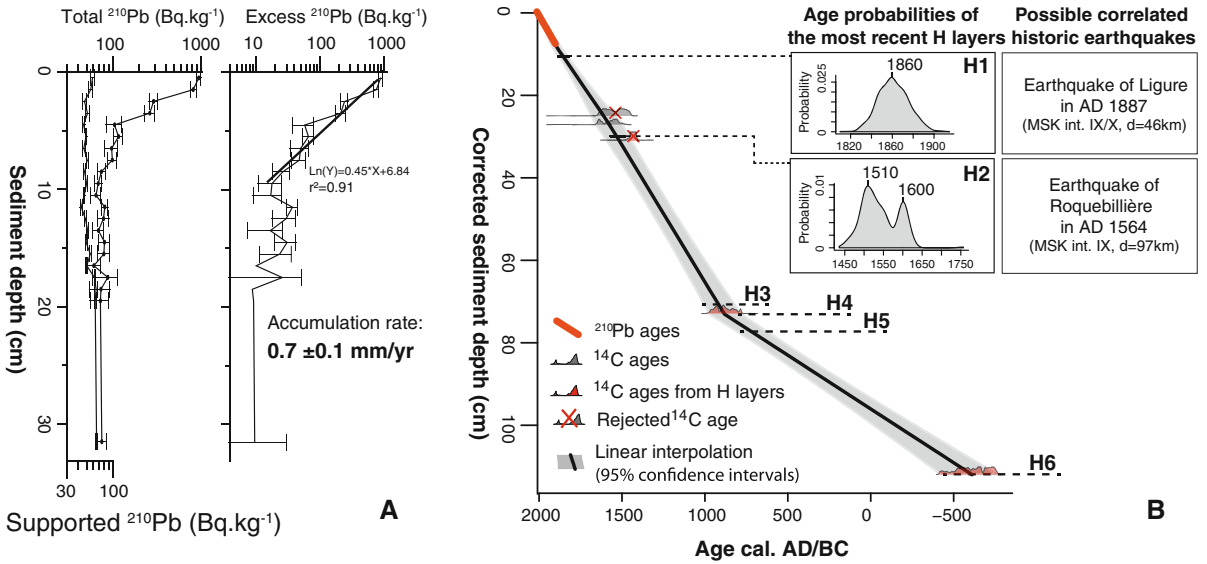

Fig. 7 **a** Total, supported, and excess ^{210}Pb versus sediment depth in core VEN09P3. **b** Age-depth relationship for core VEN09P3 and age probabilities for the H1 and H2 layers. Note that ^{14}C ages from the H layers are considered to be maximum ages (see text for details)

We combined ^{210}Pb-based ages with the five ^{14}C ages (Table 1) to construct an age-depth model for the entire VEN09P3 core (Fig. 7b). H layers are all associated with short-duration sedimentation processes and are thus considered instantaneous deposits. Hence, we excluded these deposits to construct a "corrected" depth before age-depth modeling (Arnaud et al. 2002; Wilhelm et al. 2012a). The resulting age-depth model reveals that the VEN09P3 core covers the last three millennia and provides maximum calibrated age probabilities of AD 1860 for H1, AD 1510 and 1600 for H2, AD 912 for H3, AD 890 for H4, AD 729 for H5 and BC 593 for H6 (Fig. 7b). It is, however, noteworthy that three of the five ^{14}C samples came from H layers. Because the H layers appear to result from the reworking of older sediments, these ^{14}C samples may have yielded "too-old" ages. Hence, ages on samples from H3, H4, H5 and H6 are considered maximum ages.

Discussion

Triggering processes for the three sedimentary facies

Lake Vens sediment is composed of autochthonous (silica) and allochthonous material. Along the 168-cm core length, three facies are clearly distinguishable: (1) laminae, (2) grey homogenous deposits designated 'H' layers and (3) dark sediment layers designated 'D' layers. The laminated intervals vary between high Si/K ratios, which correspond to the Si-rich diatom end-member of the D layers, and high Ca/K ratios, which correspond to the Ca-rich lithogenic end-member of the H layers. Organic matter is distributed around the limit between type II and III (Fig. 6), representing a mixture of material from algae and higher plants. The mm-scale, dark-brown laminations are considered the "sedimentary background," resulting from regular detrital input during snow melt and/or intense rainfall events and biological processes within the lake.

The D layers possess large amounts of diatoms, but little lithogenic material, according to smear slide observations and the geochemical ratios (Figs. 4 and 5). Grains are well sorted, with two dominant modes ascribed to diatom tests ($\sim$150 µm for individual diatoms and >400 µm for the colony) and a small, discrete mode ascribed to the detrital silt (40 µm). These layers also appear to be enriched in sulphur (Fig. 5) and organic matter that is dominated by algal material (Fig. 6). High sulphur concentrations could be related to authigenic pyrite formation under anoxic conditions, a consequence of increased algal productivity (Thomson et al. 2006). Concurrent increases in diatoms and algal organic matter suggest an increase

in autochthonous productivity during these two periods of deposition, linked to favourable growth conditions (water temperature, nutrient inputs) and/or reduced detrital inputs linked to decreases in the frequency and intensity of flood events and snow melts.

The H layers are dominated by erosion products from the crystalline basement, as revealed by smear slides and geochemical ratios (Figs. 4 and 5). Organic matter content is low and closer to the type III (Fig. 6), attributed to vascular plants (De Beaulieu and Jorda 1977). This is consistent with sediment dominated by the lithogenic fraction. Thus, presence of terrestrial organic matter and predominance of the lithogenic fraction in the H layers suggest their material comes predominantly from the catchment. Processes that could lead to H layer formation include erosion and transport of detrital material by a flood event or gravity reworking. With respect to floods, variations in grain size indicate two evolutionary stages, including an increase followed by a decrease in grain size, reflecting variations in stream inflow velocity during the flood event (Mulder et al. 2001; Ito et al. 2010). In some cases, the inversely graded base can be eroded during the flood event and flood deposits are thus only made up of a coarse base capped by a regular graded layer (Arnaud et al. 2002; Wilhelm et al. 2012b). Sediment features of the H layers with a well-developed homogenous layer do not appear to be associated with flood processes.

Among sediment facies associated with gravity processes, a similar type has been described as a class of lacustrine turbidites called "homogenites" or "seiche deposits" in marine (Kastens and Cita 1981; Cita and Rimoldi 1997; Rebesco et al. 2000; Çağatay et al. 2012) and lacustrine environments (Siegenthaler et al. 1987; Chapron et al. 1999; Schnellmann et al. 2005; Beck 2009). According to these authors, homogenites result indirectly from strong earthquakes. The earthquake is considered to be the factor that triggers sediment failure, evolving into mass transport or slumps, which in turn form hyperpycnal (turbidity) currents with bed-load and suspended-load (Beck 2009). The bed-load sediment would produce the sandy basal part of the H layer, whereas the suspended load would result in the main part of the H layer, characterized by homogenous grain size and composition of sediments as well as high foliation. This homogenization of the suspended-load sediment would result from oscillatory movement of the whole lake-water mass, i.e. a seiche, induced by the seismic shock. Interpretation of the H layers as earthquake-triggered deposits is also supported by the presence of microfaults, which suggest brittle deformation related to co-seismic displacements (Monecke et al. 2004). The four microfaults clearly identified by X-ray analysis are in the middle portion of the sediment core, where coring deformation is expected to be minimal. Consequently, we hypothesize that the H layers and the microfault deformation features are related to strong historic earthquake shocks, in agreement with similar microfault deformation described by Monecke et al. (2004) for laminated lake sediments of central Switzerland.

Comparison between historic earthquakes and homogenite ages

Over the past 600 years, regional earthquakes have been inventoried and are listed in databases from the BRGM (Boschi et al. 1997). In Fig. 8, the main historic seismic events are reported, with distance between Lake Vens and the earthquake epicentre and epicentre intensity. The dashed line, which represents the seismic sensitivity line, is based on previous studies of high-altitude lake sediment sequences (Nomade et al. 2005; Wilhelm et al. 2012a). This line enables identification of historic earthquakes with the potential to trigger sediment gravity reworking. Over the last 600 years, two major earthquakes in the southern Alps are highlighted. The most damaging event was the AD 1564 Roquebillière earthquake, with an estimated MSK intensity of IX–X at the epicentre (Boschi et al. 1997; Lambert and Levret 1996; Laurenti 1998). The other major event occurred in AD 1887, with an estimated epicentre MSK intensity of X along the Ligurian coastline. The two most recent H layers were dated to AD 1860 $\pm$ 30 for H1 and AD 1545 $\pm$ 30 for H2, the latter with maximum age probabilities at AD 1510 and 1600. The ages of these two H layers are well constrained by ^{210}Pb and ^{14}C dates. Good agreement between dates of the historic earthquakes and the sediment H layers suggests the H1 layer was triggered by the major 1887 Ligure earthquake and H2 was a consequence of the major 1564 Roquebillière earthquake. Historical data (compiled in www.azurseisme.com) for the AD 1887 earthquake refer to two violent events of similar intensities over a

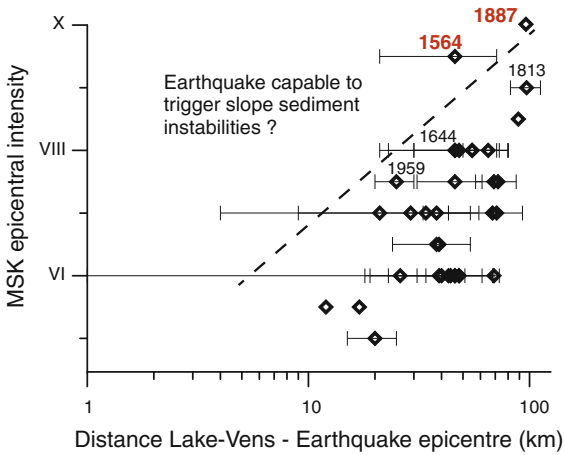

Fig. 8 Intensity versus distance diagram (MSK intensity > V and distance < 110 km) for historic earthquakes near Lake Vens. The dashed line represents the possible seismic sensitivity of Lake Vens. Dates of historic earthquakes that are probably associated with the two most recent H layers are marked in *red*

10-min interval, followed by two more minor events in the day. Consequently, we propose that the two opaque layers corresponding to H1 might correspond to this double after-shock event. One can also notice that two turbidites related to this 1887 earthquake come from a marine record of the Ligurian Margin (Hassoun et al. 2014). Sediment deposits in Lake Vens are thus a reliable recorder of large-magnitude earthquakes that occurred within ~100 km of the lake. The record suggests a recurrence time for such events in the region of about 400 years. Confirmation of this claim will require accurate dating of these earthquake-generated horizons.

Conclusions

We conducted a multi-proxy study of Lake Vens to test the paleoseismic archive potential of the lake's sediments in an area that is particularly sensitive to seismogenic hazards, the SW Alps. Sedimentological (X-ray image, grain-size distribution) and geochemical (major elements and organic matter) analyses show that Lake Vens sediment is made of two main components: 1) terrigenous material sourced from the watershed (minerals and organic matter) and 2) authigenic material, mainly diatom frustules. The sediment is composed of silty, irregular, mm-scale laminae, with two layers characterised by high numbers of diatom frustules. Striking sedimentological features include six homogenous deposits or 'homogenites' that are interbedded into the sedimentary background. A coarse base, a main layer characterized by homogenous grain size and geochemistry, and a fine-whitish clay cap characterize all these deposits. Homogenous grain size and Ca/K ratios with increased foliation are the main characteristics that suggest these layers are "homogenite" type, which have been described by several authors as resulting from strong earthquakes. The age model, established using ^{210}Pb and ^{14}C dates, indicates that core VEN09P3 covers the last 2,600 years. The H1 layer may correspond to gravity reworking of slope sediment, as a response to the major Ligure earthquake in AD 1887. The H2 layer may have been caused by the AD 1564 Roquebillière earthquake.

The sediment sequence of Lake Vens probably possesses information that can be used to establish regional earthquake events throughout the Holocene. Initial findings suggest a recurrence of major earthquakes every ~400 years, but additional cores from Lake Vens and further ^{14}C dating will be needed to confirm this. Furthermore, sediment data from other lakes in the region could be studied to confirm the hypotheses and better locate the epicentres of past earthquakes.

Acknowledgments This work was supported by a Geoazur BQR internal grant and University of Savoie's AAP-2013-AGRASM2 Grant dedicated to AMS sedimentological applications. Gravity Coring was achieved with the support of the Edytem coring facility. We thank E. Malet and C. Pignol for their support of field logistics during the Dolce Vita campaign, and thank Isabelle Billy for the XRF core-scanner measurements. The authors also thank Nicolas Thouveny for providing access to facilities at the CEREGE paleomagnetic laboratory (Aix-Marseille University), R. Lemée for diatom pictures, J.L. Reiss for discussion of the chronology and J.R. Disnar for organic matter analyses. Thanks to an anonymous reviewer and to Maarten Van Daele for their constructive comments. All "SacA" ^{14}C samples were measured in the Saclay LMC14 laboratory under the auspices of the national program "Artemis." The authors thank J.P. Dumoulin and T. Goslar from Poznan Radiocarbon Laboratory for help with ^{14}C sample analysis and interpretation.

References

Alfaro P, Estevez A, Moretti M, Soria JM (1999) Sedimentary deformation structures interpreted as seismites in the Quaternary of the Low Segura basin (Eastern Betic Cordillera). C R Acad Sci Serie IIa Sci Terre 3281:17–22

Ambraseys NN (1988) Engineering seismology. Earthq Eng Struct Dynam 17:1–105
Arnaud F, Lignier V, Revel M, Desmet M, Beck C, Pourchet M, Charlet F, Trentesaux A, Tribovillard N (2002) Flood and earthquake disturbance of 210Pb geochronology (Lake Anterne, NW Alps). Terra Nova 14:225–232
Bauve V, Rolland Y, Sanchez G, Giannerini G, Schreiber D, Corsini M, Perez JL, Romagny A (2012) Pliocene to Quaternary deformation in the Var Basin (Nice, SE France) and its interpretation in terms of "slow-active" faulting along the Alpine Front. Swiss J Geosci 105:361–376
Beck C (2009) Late Quaternary lacustrine paleo-seismic archives in north-western Alps: examples of earthquake-origin assessment of sedimentary disturbances. Earth Sci Rev 96:327–344
Beck C, Manalt F, Chapron E, Van Rensbergen P, De Batist M (1996) Enhanced seismicity in the early post-glacial period: evidence from the post-Würm sediments of Lake Annecy, northwestern Alps. J Geodyn 22:155–171
Blaauw M (2010) Methods and code for 'classical' age-modelling of radiocarbon sequences. Quat Geochronol 5:512–518
Boschi E, Guidoboni E, Ferrari G, Valensise G, Gasperini P (1997) The catalogue of strong Italian Earthquakes on the web. http://storing.ingrm.it/cft/
Çağatay MN, Erel L, Bellucci LG, Polonia A, Gasperini L, Eriş KK, Sancar Ü, Biltekin D, Uçarkuş G, Ülgen UB, Damci E (2012) Sedimentary earthquake records in the İzmit Gulf, Sea of Marmara, Turkey. Sediment Geol 282:347–359
Campos C, Beck C, Crouzet C, Demory F, Van Welden A, Eris K (2013) Deciphering hemipelagites from homogenites through anisotropy of magnetic susceptibility. Paleoseismic implications (Sea of Marmara and Gulf of Corinth). Sediment Geol 292:1–14
Chapron E, Beck C, Pourchet M, Deconinck JF (1999) 1822 AD earthquake-triggered homogenite in Lake Le Bourget (NW Alps). Terra Nova 11:86–92
Cita MB, Rimoldi B (1997) Geological and geophysical evidence for a Holocene tsunami deposit in the eastern Mediterranean deep-sea record. J Geodyn 24:293–304
Courboulex F, Larroque C, Deschamps A, Gélis C, Charreau J, Stéphan JF (2003) An unknown active fault revealed by microseismicity in the south-east of France. Geophys Res Lett 30:1782
Darnault R, Rolland Y, Bourlès D, Braucher R, Sanchez G, Revel M, Bouissou S (2012) Timing of the last deglaciation revealed by receding glaciers at the Alpine-scale: impact on mountain geomorphology. Quat Sci Rev 31:127–142
De Beaulieu JL, Jorda M (1977) Tardiglaciaire et postglaciaire des Alpes de Haute Provence. Bull Assoc Fr Etud Quat 3:3–15
Disnar JR, Guillet B, Keravis D, Di-Giovanni C, Sebag D (2003) Soil organic matter (SOM) characterization by Rock-Eval pyrolysis: scope and limitations. Org Geochem 34:327–343
Espitalie J, Deroo G, Marquis F (1985) La pyrolyse Rock-Eval et ses applications. Première partie. Rev Inst Fr Pétrole 40:563–579
Gaggeler H, Von Gunten HR, Nyffeler U (1976) Determination of 210Pb in lake sediments and in air samples by direct gamma-ray measurement. Earth Planet Sci Lett 33:119–121
GEMGEP report (2005) http://www.planseisme.fr/IMG/pdf/Rapport_GEMGEP_Nice_-_partie_2.pdf
Goldberg DE (1963) Geochronology with 210Pb. In: IAEA (ed) Symposium on radioactive dating. pp 121–131
Hassoun V, Martin J, Migeon S, Larroque C, Cattaneo A, Eriksson M, Sanchez-Cabeza JA, Mercier de Lepinay B, Liong Wee Kwong L, Levy I, Heimbürger LE, Miquel JC (2014) Searching for the Record of Historical Earthquakes, Floods and Anthropogenic Activities in the Var Sedimentary Ridge (NW Mediterranean). In: S. Krastel et al. (ed) Submarine Mass Movements and Their Consequences, Advances in Natural and Technological Hazards Research vol 37, p 571–581
Ito T, Iwamoto H, Kamiya K, Fukushima T, Kumon F (2010) Use of flood chronology for detailed environmental analysis: a case study of Lake Kizaki in the northern Japanese Alps, central Japan. Environ Earth Sci 60:1607–1618
Jenatton L, Guiguet R, Thouvenot F, Daix N (2007) The 16,000 event 2003–2004 earthquake swarm in Ubaye (French Alps). J Geophys Res 112:304
Jewell HE, Ettensohn FR (2004) An ancient seismite response to Taconian far-field forces: the Cane Run Bed, Upper Ordovician (Trenton) Lexington Limestone, Central Kentucky (USA). J Geodyn 37:487–511
Kastens K, Cita MB (1981) Tsunami-induced sediment transport in the abyssal Mediterranean Sea. Geol Soc Am Bull 92:845–857
Lambert J, Levret A (1996) Mille ans de séismes en France. Ouest Editions Presses Académiques, Nantes
Larroque C, Delouis B, Hippolyte JC, Deschamps A, Lebourg T, Courboulex F, Bellier O (2011) Joint multidisciplinary study of the Saint-Sauveur–Donareo fault (lower Var valley, French Riviera): a contribution to seismic hazard assessment in the urban area of Nice. Bull Soc Geol Fr 182:323–336
Laurenti A (1998) Les tremblements de terre des Alpes Maritimes. Serre Editeur, Nice
Meyers PA, Lallier-Vergès E (1999) Lacustrine sedimentary organic matter records of Late Quaternary paleoclimates. J Paleolimnol 21:345–372
Migeon S, Weber O, Faugeres JC, Saint-Paul J (1999) SCOPIX: a new X-ray imaging system for core analysis. Geo-Mar Lett 18:251–255
Monecke K, Anselmetti F, Becker A, Sturm M, Giardini D (2004) Signature of historic earthquakes in lake sediments in Central Switzerland. Tectonophysics 394:21–40
Mulder T, Migeon S, Savoye B, Faugères JC (2001) Inversely graded turbidite sequences in the Deep Mediterranean: a record of deposits from flood-generated turbidity currents. Geo-Mar Lett 21:86–93
Nomade J, Chapron E, Desmet M, Reyss JL, Arnaud F, Lignier V (2005) Reconstructing historical seismicity from lake sediments (Lake Laffrey, Western Alps, France). Terra Nova 17:350–357
Obermeier S (1996) Use of liquefaction-induced features for paleoseismic analysis-An overview of how seismic liquefaction features can be distinguished from other features and how their regional distribution and properties of source sediment can be used to infer the location and strength of Holocene paleo-earthquakes. Eng Geol 44:1–76

Plaziat JC, Ahmamou M (1998) Mechanic processes active in seismites: their identification and tectonic significance in the Pliocene basin of the Sais of Fes and Meknes (Morocco). Geodin Acta 11:183–203

Rebesco M, Della Vedova B, Cernobori L, Aloisi G (2000) Acoustic facies of Holocene megaturbidites in the Eastern Mediterranean. Sedim Geol 135:65–74

Reimer PJ, Baillie MGL, Bard E, Bayliss A, Beck JW, Blackwell PG (2009) IntCal09 and Marine09 radiocarbon age calibration curves, 0–50,000 years cal BP. Radiocarbon 51:1111–1150

Rodriguez-Pascua MA, Calvo JP, De Vicente G, Gomez-Gras D (2000) Soft-sediment deformation structures interpreted as seismites in lacustrine sediments of the Prebetic Zone, SE Spain, and their potential use as indicators of earthquake magnitudes during the Late Miocene. Sedim Geol 135:117–135

Sanchez G, Rolland Y, Corsini M, Braucher R, Bourlès D, Arnold M, Aumaître G (2010a) Relationships between tectonics, slope instability and climate change: cosmic ray exposure dating of active faults, landslides and glacial surfaces in the SW Alps. Geomorphology 117:1–13

Sanchez G, Rolland Y, Schreiber D, Giannerini G, Corsini M, Lardeaux JM (2010b) The active fault system of SW Alps. J Geodyn 49:296–302

Sanchez G, Rolland Y, Corsini M, Jolivet M, Brichaud S, Carter A (2011a) Exhumation controlled by transcurrent tectonics: the Argentera-Mercantour massif (SW Alps). Terra Nova 23:116–126

Sanchez G, Rolland Y, Corsini M, Oliot E, Goncalves P, Schneider J, Verati C, Lardeaux JM, Marquer D (2011b) Dating low-temperature deformation by 40Ar/39Ar on white mica, insights from the Argentera–Mercantour Massif (SW Alps). Lithos 125:521–536

Schnellmann M, Anselmetti FS, Giardinio D, McKenzie JA (2005) Mass movement-induced fold-and-thrust belt structures in unconsolidated sediments in Lake Lucerne (Switzerland). Sedimentology 52:271–289

Seilacher A (1969) Fault-graded beds interpreted as seismites. Sedimentology 13:155–159

Shiki T, Kumon F, Inouchi Y, Kontani Y, Sakamoto T, Tateishi M, Matsubara H, Fukuyama K (2000) Sedimentary features of the seismo-turbidites, Lake Biwa, Japan. Sedim Geol 135:37–50

Siegenthaler C, Finger W, Kelts K, Wang S (1987) Earthquake and seiche deposits in Lake Lucerne, Switzerland. Eclogae Geol Helv 80:241–260

Sims JD (1973) Earthquake-induced structures in sediments of Van Norman Lake, San Fernando, California. Science 182:161–163

Sims JD (1975) Determining earthquake recurrence intervals from deformational structures in young lacustrine sediments. Tectonophysics 29:144–152

Strasser M, Anselmetti FS, Donat F, Giardini D, Schnellmann M (2006) Magnitudes and source areas of large prehistoric northern Alpine earthquakes revealed by slope failures in lakes. Geology 12:1005–1008

Thomson J, Croudace IW, Rothwell RG (2006) A geochemical application of the ITRAX scanner to a sediment core containing eastern Mediterranean sapropel units. In: Rothwell G (ed) New techniques in sediment core analysis, vol 267. Geological Society, London, Special Publications, pp 65–77

Wilhelm B, Arnaud F, Enters D, Allignol F, Legaz A, Magand O, Revillon S, Giguet-Covex C, Malet E (2012a) Does global warming favour the occurrence of extreme floods in European Alps? First evidences from a NW Alps proglacial lake sediment record. Clim Change 113:563–581

Wilhelm B, Arnaud F, Sabatier P, Brisset E, Chaumillon E, Disnar JP, Guiter F, Malet E, Reyss JL, Tachikawa K, Bard E, Delannoy JL (2012b) 1500 years of extreme precipitation patterns and forcing over the Mediterranean French Alps. Quat Res 78:1–12

Wilhelm B, Arnaud F, Sabatier P, Magand O, Chapron E, Courp T, Tachikawa K, Fanget B, Malet E, Pignol C, Bard E, Delannoy JJ (2013) Palaeoflood activity and climate change over the last 1400 years recorded by lake sediments in the NW European Alps. J Quat Sci 28(2):189–199